



Originally published as:

Li, X., Zus, F., Lu, C., Ning, T., Dick, G., Ge, M., Wickert, J., Schuh, H. (2015): Retrieving high-resolution tropospheric gradients from multiconstellation GNSS observations. - *Geophysical Research Letters*, 42, 10, p. 4173-4181.

DOI: <http://doi.org/10.1002/2015GL063856>

RESEARCH LETTER

10.1002/2015GL063856

Key Points:

- Retrieving high-resolution tropospheric gradients from multi-GNSS observations
- Gradients agree well with weather models and other meteorological observations
- Compared to GPS only, the correlation is improved significantly up to 20–35%

Supporting Information:

- Text S1
- Figure S1

Correspondence to:

C. Lu,
cuixian@gfz-potsdam.de

Citation:

Li, X., F. Zus, C. Lu, T. Ning, G. Dick, M. Ge, J. Wickert, and H. Schuh (2015), Retrieving high-resolution tropospheric gradients from multiconstellation GNSS observations, *Geophys. Res. Lett.*, 42, 4173–4181, doi:10.1002/2015GL063856.

Received 14 MAR 2015

Accepted 28 APR 2015

Accepted article online 29 APR 2015

Published online 20 MAY 2015

Retrieving high-resolution tropospheric gradients from multiconstellation GNSS observations

Xingxing Li¹, Florian Zus¹, Cuixian Lu¹, Tong Ning¹, Galina Dick¹, Maorong Ge¹, Jens Wickert¹, and Harald Schuh¹
¹German Research Centre for Geosciences, Potsdam, Germany

Abstract The developing multi-Global Navigation Satellite Systems (GNSS) constellations have the potential to provide accurate high-resolution tropospheric gradients. Such data, closely linked to strong humidity gradients accompanying severe weather phenomena, are considered a new important data source for meteorological studies, e.g., nowcasting of severe rainfall events. Here we describe the development of a multi-GNSS processing system for the precise retrieval of high-resolution tropospheric gradients. The retrieved products were validated by using independent water vapor radiometer (WVR) observations and numerical weather model (NWM) data. The multi-GNSS high-resolution gradients agree well with those, derived from NWM and WVR, especially for the fast-changing peaks which were mostly associated with synoptic fronts. Compared to GPS-only gradients, the correlations with the validation data are significantly improved up to 20–35%. The new data product has significant potential to improve numerical weather prediction and to advance meteorological studies.

1. Introduction

Atmospheric water vapor is highly variable in space and time depending on the complex interplay of several phenomena like convection, precipitation, turbulence etc. [Gendt et al., 2004]. The distribution of water vapor and the development of precipitation systems mutually affect each other [Shoji, 2013]. Remarkable progress in using ground-based GPS receivers for remote sensing of the atmospheric water vapor has been achieved during the last decades [Bevis et al., 1992; Rocken et al., 1997; Fang et al., 1998; Gendt et al., 2004; Li et al., 2014] as GPS has several significant advantages of low-operating expense, all-weather capability, and high spatiotemporal resolution. The zenith total delay (ZTD), which is closely related to the integrated water vapor above the station, is the basic observable in GPS meteorology [Bevis et al., 1992]. Currently, the GPS-derived ZTD data are assimilated operationally at several weather agencies worldwide [e.g., Poli et al., 2007]. These centers have shown the benefit of GPS ZTD for short-term severe precipitation forecast [Karabatic et al., 2011; Dousa and Vlacovic, 2014].

It is obvious that the ZTD from a single station supplies vertically integrated information on the atmospheric refractivity but does not contain information about its horizontal distribution. The horizontal gradients provide additional information to describe tropospheric asymmetry [Davis et al., 1993]. This asymmetry is typically most significant in the vicinity of strong horizontal humidity gradients, accompanying severe weather phenomena [Miyazaki et al., 2003]. The ability to sense troposphere gradients potentially increases the useful meteorological information content. Especially, high-resolution gradient parameters will help with nowcasting of severe rainfall because the tropospheric gradient is higher correlated with strong rainfall than precipitable water vapor [Shoji, 2013].

The estimation of horizontal atmospheric gradients, in addition to zenith delays, is a strategy now commonly used in geodetic GPS processing. This strategy compensates for inhomogeneities in the atmospheric water vapor distribution above GPS sites and has shown to increase the positioning precision [Bar-Sever et al., 1998; Miyazaki et al., 2003]. Estimation of piecewise gradient parameters on a daily basis has been a common practice in order to reduce the number of epoch-wise estimated parameters and to prevent large variations and jumps in estimated gradients [Meindl et al., 2004]. In the recent IGS (International Global Navigation Satellite Systems (GNSS) Service) reprocessing campaign, the most of the analysis centers (e.g., Center for Orbit Determination in Europe (CODE), GeoForschungsZentrum (GFZ), European Space Agency (ESA), Massachusetts Institute of Technology (MIT)) estimated pairs of horizontal delay

gradient parameters in north and east direction for each station in intervals of 24 h and the gradient estimates represent averages over longer time spans, except that Jet Propulsion Laboratory used the random walk process imposed by a rather tight time correlation (<http://acc.igs.org/reprocess2.html>). However, the numerical weather model (NWM)-based investigation results show that, depending on the location and season, gradients may vary several millimeters over a much shorter period of time than 24 h.

The accuracy of high-resolution gradient estimates is probably limited by the geometry of the GPS satellites, i.e., the insufficient and inhomogeneous coverage of GPS satellites. Generally speaking, about 6–12 GPS satellites could be observed simultaneously at one site [Li *et al.*, 2015a]. This might be insufficient for estimating water vapor gradients. Fortunately, the satellite navigation is undergoing dramatic changes with the rapid development of multiconstellation GNSS. At the moment, more than 70 satellites are already in view (32 GPS, 24 GLONASS, 14 BeiDou, and 4 Galileo), and about 120 satellites will be available once all four systems are fully deployed in the next few years. Many GPS networks are now being upgraded to multi-GNSS observation networks, e.g., the IGS MGEX (The Multi-GNSS Experiment) network which includes more than 100 stations [Montenbruck *et al.*, 2014]. This brings great opportunities and potential for both geodetic and geophysical applications. It is expected that multi-GNSS processing with more satellites and better geometry can contribute to stabilize high-resolution gradient estimation [Li *et al.*, 2015b].

In this contribution, we develop a multi-GNSS processing for the estimation of high-resolution tropospheric gradients based on the single-receiver PPP (precise point positioning) [Zumberge *et al.*, 1997; Li *et al.*, 2013] technique. The observations from the globally distributed MGEX stations are processed, and the high-resolution multi-GNSS gradients are retrieved. The performance of the retrieved gradients was validated by using independent water vapor radiometer (WVR) observations and estimates from NWM, and the benefit of multi-GNSS fusion to high-resolution tropospheric gradients was demonstrated.

2. Data Analysis

2.1. Retrieving Multi-GNSS Gradient

In the PPP processing, precise satellite orbits and clocks are fixed to previously determined values. The station coordinates can usually be well known in meteorological applications. Therefore, the PPP model for multi-GNSS processing (here GPS, Global Navigation Satellite System (GLONASS), Galileo, and BeiDou) can be formulated as [Li *et al.*, 2015b]

$$\begin{cases} l_{r,j}^G = t_r + \lambda_{jG}(b_{rG,j} - b_j^G) + \lambda_{jG}N_{r,j}^G - \kappa_{jG} \cdot I_{r,1}^G + T_r + \varepsilon_{r,j}^G \\ l_{r,j}^{R_k} = t_r + \lambda_{jR_k}(b_{rR_k,j} - b_j^R) + \lambda_{jR_k}N_{r,j}^{R_k} - \kappa_{jR_k} \cdot I_{r,1}^R + T_r + \varepsilon_{r,j}^{R_k} \\ l_{r,j}^E = t_r + \lambda_{jE}(b_{rE,j} - b_j^E) + \lambda_{jE}N_{r,j}^E - \kappa_{jE} \cdot I_{r,1}^E + T_r + \varepsilon_{r,j}^E \\ l_{r,j}^C = t_r + \lambda_{jC}(b_{rC,j} - b_j^C) + \lambda_{jC}N_{r,j}^C - \kappa_{jC} \cdot I_{r,1}^C + T_r + \varepsilon_{r,j}^C \end{cases} \quad (1)$$

$$\begin{cases} p_{r,j}^G = t_r + c \cdot d_{rG} + \kappa_{jG} \cdot I_{r,1}^G + T_r + e_{r,j}^G \\ p_{r,j}^{R_k} = t_r + c \cdot d_{rR_k} + \kappa_{jR_k} \cdot I_{r,1}^R + T_r + e_{r,j}^{R_k} \\ p_{r,j}^E = t_r + c \cdot d_{rE} + \kappa_{jE} \cdot I_{r,1}^E + T_r + e_{r,j}^E \\ p_{r,j}^C = t_r + c \cdot d_{rC} + \kappa_{jC} \cdot I_{r,1}^C + T_r + e_{r,j}^C \end{cases} \quad (2)$$

where r and j refer to receiver and frequency, respectively. The indices G , R , E , and C refer to the GPS, GLONASS, Galileo, and BeiDou satellites, respectively; R_k denotes the GLONASS satellite with frequency factor k ; $l_{r,j}$ and $p_{r,j}$ denote “observed minus computed” phase and pseudorange observables; t_r is the receiver clock bias; $N_{r,j}$ is the integer ambiguity; b_j is the uncalibrated phase delays; λ_j is the wavelength; the ionospheric delays I_j at different frequencies can be expressed as $I_j = \kappa_j \cdot I_1$, $\kappa_j = \lambda_j^2 / \lambda_1^2$; T_r is the slant tropospheric delay; and $e_{r,j}$ and $\varepsilon_{r,j}$ denote measurement noise and multipath. The phase center offsets and variations, tidal loading, and phase wind-up can be corrected according to the existing models [Li *et al.*, 2013]. Due to the different frequencies and signal structure of the individual GNSS, the code biases d_{rG} , d_{rR_k} , d_{rE} , and d_{rC} are different in one multi-GNSS receiver. These intersystem biases (ISB), and interfrequency biases (IFB) of the GLONASS satellites with different frequency factors, must be carefully considered in a combined processing of multi-GNSS observations.

To account for both homogeneity and inhomogeneity of the troposphere, the complete model for the line-of-sight delay T_r is [Davis et al., 1993]

$$T_r^s = Mh_r^s \cdot Zh_r + Mw_r^s \cdot Zw_r + Mw_r^s \cdot \cot(e) \cdot (G_N \cdot \cos(a) + G_E \cdot \sin(a)) \quad (3)$$

The zenith hydrostatic delay (ZHD) Zh_r can be computed rather accurately using the Saastamoinen model [Saastamoinen, 1973] and meteorological data, the zenith wet delay (ZWD) Zw_r and horizontal gradients G_N and G_E in north and east directions have to be estimated as parameters. Mh_r^s and Mw_r^s are the hydrostatic and wet coefficients of the global mapping function (GMF) [Böhm et al., 2006]; e and a are the elevation and azimuth angles. In our multi-GNSS PPP-based tropospheric monitoring, the estimated parameters vector \mathbf{X} can be expressed as

$$\mathbf{X} = \left(Zw_r \ G_N \ G_E \ t_r \ d_{rE} \ d_{rC} \ d_{rRk} \ \mathbf{I}_{r,1}^s \ \bar{\mathbf{N}}_r^s \right)^T \quad (4)$$

$$\bar{\mathbf{N}}_r^s = \mathbf{N}_r^s + \mathbf{b}_r + \mathbf{b}^s \quad (5)$$

All the observations from different GNSS (four systems) are processed together in one weighted least squares estimator to perform a rigorous multi-GNSS analysis. The receiver clock bias t_r is estimated as white noise. The ISB and IFB parameters are estimated on a daily basis. We set up the code bias parameters for each system and each GLONASS frequency, and the code bias for GPS satellites is set to zero in order to eliminate the singularity between receiver clock and code bias parameters. This means that all estimated biases of other systems are relative to the biases for the GPS satellites. The phase delays b_j will be absorbed by phase ambiguity parameters, and the phase ambiguities $\bar{\mathbf{N}}_r^s$ are estimated as constant for each continuous arc. The ionospheric delays $\mathbf{I}_{r,1}^s$ are taken as estimated parameters for each satellite and at each epoch by using dual-frequency raw phase and pseudorange observations. The Saastamoinen model is used to calculate the a priori ZHD, and the a priori values for gradients are zero. The GMF was used to calculate the hydrostatic and wet mapping functions. The tropospheric zenith wet delay and associated north and east horizontal gradients are modeled as piecewise constant parameters in intervals of 1 or 2 h for high-resolution tropospheric products. A very loose relative constraint of about $30 \text{ mm}/\sqrt{h}$ is imposed for gradient and ZWD parameters to track fast-changing gradients. The elevation dependent weighting strategy and a cutoff elevation angle of 7° are applied.

2.2. Gradients Derived From the NWM

Given numerical weather model data and the ray trace algorithm proposed by Zus et al. [2014], tropospheric delays can be computed with high speed and precision for any elevation and azimuth angle. We utilize the pressure, temperature, and specific humidity fields from the ECMWF (European Centre for Medium-Range Weather Forecasts) operational analysis (<http://www.ecmwf.int/>) available every 6 h (0, 6, 12, and 18 UTC) with a horizontal resolution of $1^\circ \times 1^\circ$ on 137 model levels extending from Earth's surface to 80 km. For any station, tropospheric gradients are estimated from tropospheric delays as follows. At first, a set of azimuth dependent tropospheric delays is computed; the spacing in azimuth is 30° , and the elevation angles are 3° , 5° , 7° , 10° , 15° , 20° , 30° , 50° , 70° , and 90° . Second, under the assumption of a spherically layered atmosphere, the corresponding set of azimuth independent tropospheric delays is computed. Third, the differences between azimuth dependent and azimuth independent tropospheric delays are computed. Finally, the computed residuals and the gradient mapping function proposed by Chen and Herring [1997] are used to estimate by least squares fitting the tropospheric gradients. We note that dry and wet delays are computed separately as well to allow for the separate estimation of dry and wet gradients.

2.3. WVR Gradient Retrieval

The Onsala Space Observatory is operating a WVR, which carries measurements in a dual frequency (21.0 and 31.4 GHz) and is mounted less than 10 m away from the multi-GNSS station, ONS1 with a height difference less than 1 m. The WVR is operated continuously in a so-called "sky-mapping" mode, which corresponds to a repeated cycle (every 15 min) of 60 observations spread over the sky with the lowest elevation angle of 20° , typically resulting in 6000–9000 measurements per day. The WVR line-of-sight wet delays were inferred from the sky brightness temperatures using tip curves for calibration as described by Elgered and Jarlemark [1998]. The WVR does not produce gradient estimates directly. All the line-of-sight observations acquired were used

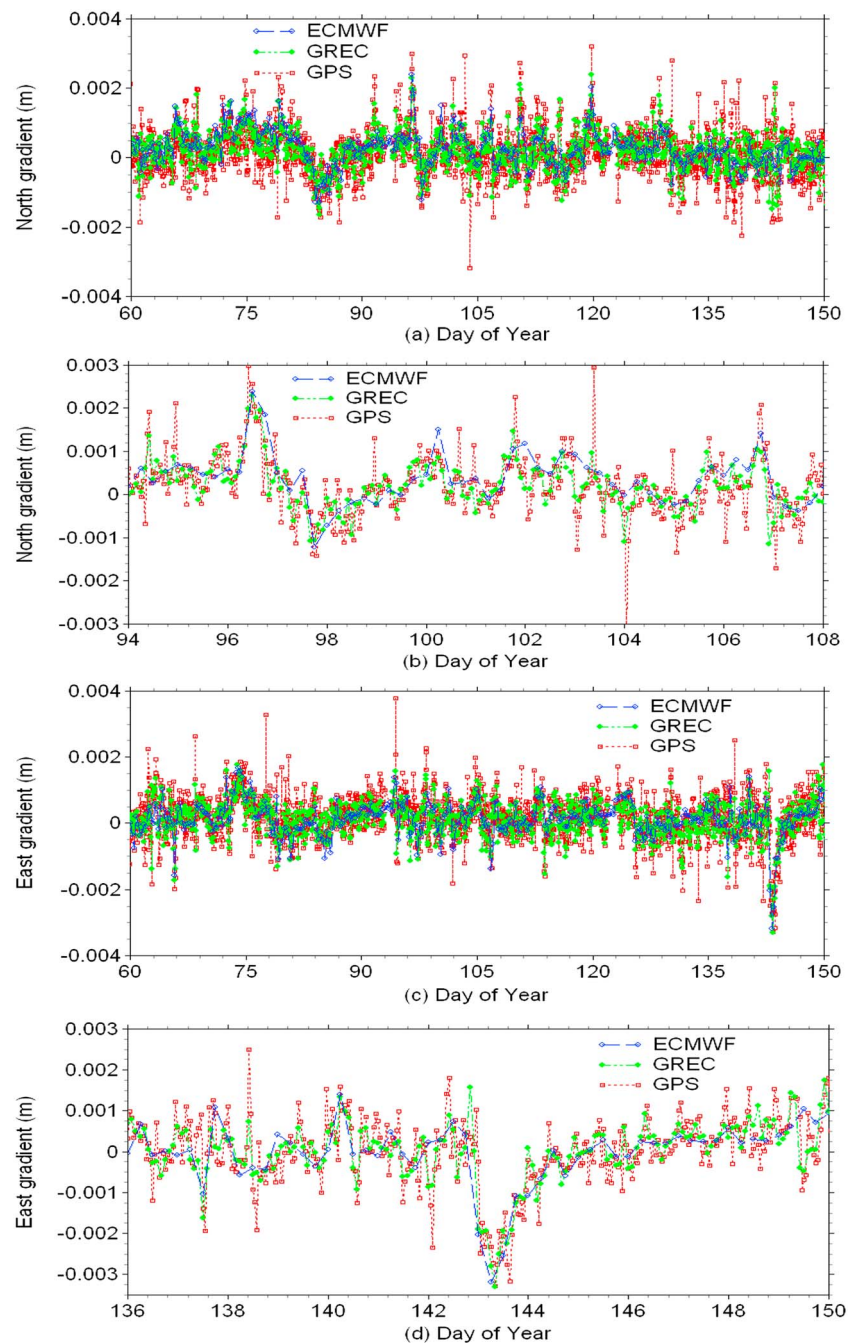


Figure 1. Tropospheric horizontal gradients retrieved from GPS-only and multi-GNSS combined (G + R + E + C) solutions at the station ONS1 (57.40°N, 11.93°W, Sweden, Europe) for a period of 3 months (March, April, and May, day of year 60 to 150 in 2014). The tropospheric gradients derived from ECMWF are used for validation as an independent reference. (a) The north-south total gradients of 3 months from GPS-only, multi-GNSS, and ECMWF solutions are shown by the red, green, and blue symbols, respectively. (b) The enlarged view of a north gradient peak during the period DOY 94–108. (c) The east-west total gradients of 3 months. (d) The enlarged view of an east gradient peak during the period DOY 136–150.

to estimate the zenith delays as well as the tropospheric gradients with an in-house software package. The tropospheric gradients are estimated using the model presented by equation (3). This process is analogous to the GNSS solution process, and a least squares estimator was used to solve the gradients for different time scales, e.g., 15 min, 1 h, or 2 h. The retrieved WVR gradients then can be used to validate the GNSS-based estimates, establishing a direct evaluation of performance through a comparison with an independent

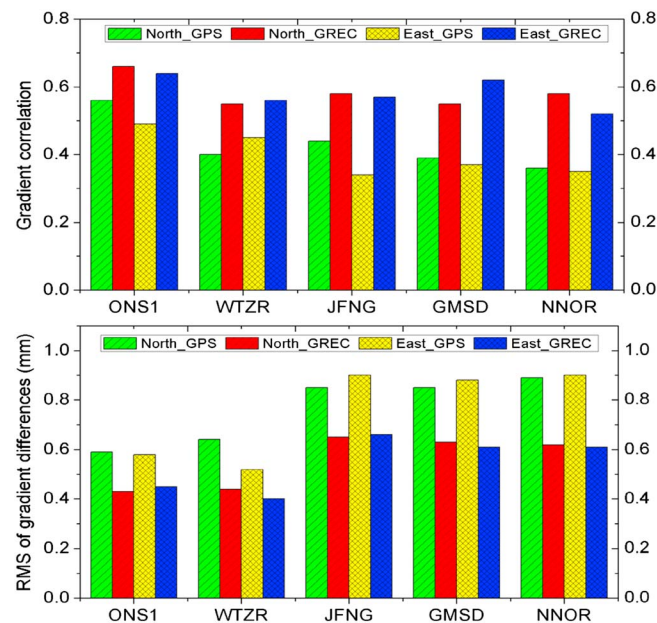


Figure 2. The correlation coefficients and RMS values of the tropospheric gradients for GPS-only and multi-GNSS solutions with respect to the ECMWF solution.

shown in Figure 1. The tropospheric gradients derived from ECMWF with time resolution of 6 h interval are also shown for validation as an independent reference. In the Figure 1a, the north-south gradients of 3 months from multi-GNSS and ECMWF solutions are shown by the green and blue symbols, respectively. We can see that the multi-GNSS gradients agree quite well with the ECMWF gradients, especially for spike-shaped peaks which were mostly associated with synoptic fronts. Figure 1b shows the enlarged view of a gradient peak during the period of day of year (DOY) 94–108. We calculated the correlation coefficient between the multi-GNSS and ECMWF gradients, and it is 0.66. Such an excellent agreement implies that the troposphere gradients can be captured accurately by the high-resolution multi-GNSS estimates.

The tropospheric gradients, retrieved from GPS-only solutions with time resolution of 1 h interval, are also shown by the red symbols for the comparison. GPS gradients show larger noise and jumps, suggesting that a lower number of GPS satellites and poor geometry condition limits the quality of gradient estimates. Such instability is not good for meteorological application which requires consistently accurate solutions. It is clearly observed that high-resolution gradient estimates with multi-GNSS processing are much more stable than those based only on GPS, and sudden jumps observed in GPS-only solutions are significantly reduced in multi-GNSS estimates because of the higher number of GNSS satellites and improved geometry coverage. The correlation coefficient between the GPS-only and ECMWF gradients is 0.54. Compared to GPS-only estimates, the correlation is improved about 22.2% by multi-GNSS processing. We also calculate the root-mean-square (RMS) values of the gradient differences for GPS-only and multi-GNSS solutions with respect to the ECMWF solution, and they are 0.59 and 0.43, respectively. An improvement of about 27.1% is achieved by the multi-GNSS processing.

The east gradients of the corresponding 3 months are compared in Figure 1c, and the enlarged view of an east gradient peak during the period DOY 136–150 is also shown in Figure 1d. Excellent agreement between multi-GNSS and ECMWF gradients can be clearly observed. Compared to GPS-only estimates, the correlation coefficient between the multi-GNSS and ECMWF gradients is increased from 0.49 to 0.64, about a 30.6% improvement. The RMS value is reduced by about 22.4%, from 0.58 to 0.45.

The correlation coefficients and RMS values of the tropospheric gradients for GPS-only and multi-GNSS solutions with respect to the ECMWF solution at several four-system stations are compared in Figure 2. It can be seen that the multi-GNSS fusion can significantly increase the correlation coefficients of high-resolution gradient estimation in both north and east components. The correlation coefficients for the multi-GNSS

technique. It should be noted that the WVR data only provide wet gradients, while the other two techniques, GNSS and ECMWF, include both the wet and dry gradients.

3. Validations With ECMWF

In order to assess the performance of high-resolution tropospheric gradients retrieved from the multi-GNSS processing, we analyzed the multi-GNSS observations from the IGS MGEX stations based on the PPP technique as described in section 2. Taking the four-system station ONS1 (Sweden, 57.40°N, 11.93°W) as a typical example, the tropospheric horizontal gradients retrieved from four-system combined (called as GREC, i.e., GPS, GLONASS, Galileo, and BeiDou) solutions with time resolution of 1 h interval for a period of 3 months (March, April, and May, day of year 60 to 150 in 2014) are

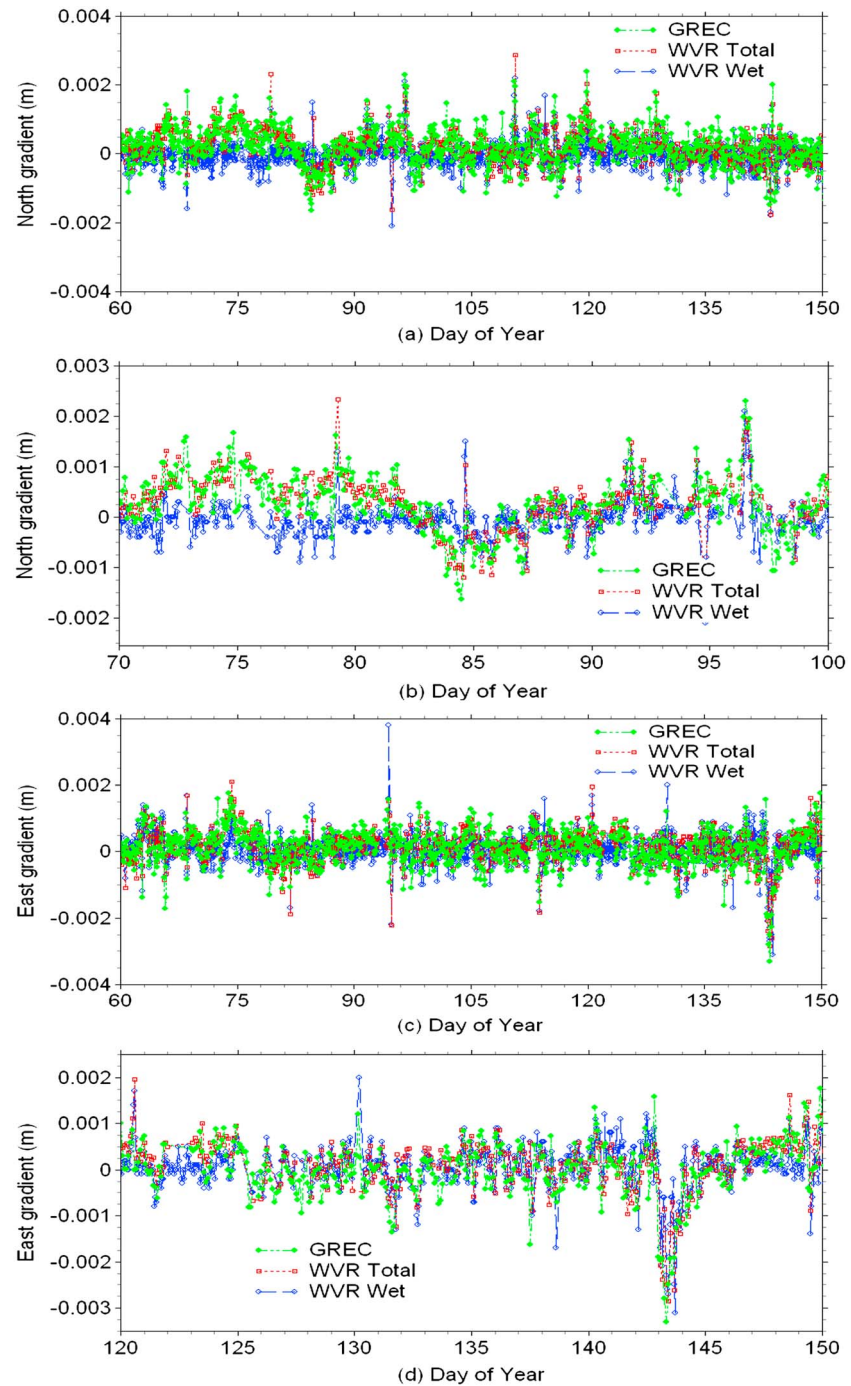


Figure 3. Tropospheric horizontal gradients retrieved from multi-GNSS combined solution at the station ONS1 and the collocated WVR measurements for a period of 3 months (March, April, and May, day of year 60 to 150 in 2014). As the gradients from the WVR are wet-only gradients and do not contain hydrostatic parts, the ECMWF dry gradients are used to convert WVR wet gradients to total gradients. (a) The multi-GNSS, WVR wet-only, and WVR total (with ECMWF dry parts as corrections) gradients of 3 months in north-south component are shown by the green, blue, and red symbols, respectively. (b) The enlarged view of a north gradient peak during the period DOY 70–100. (c) The east-west gradients of 3 months. (d) The enlarged view of an east gradient peak during the period DOY 120–150.

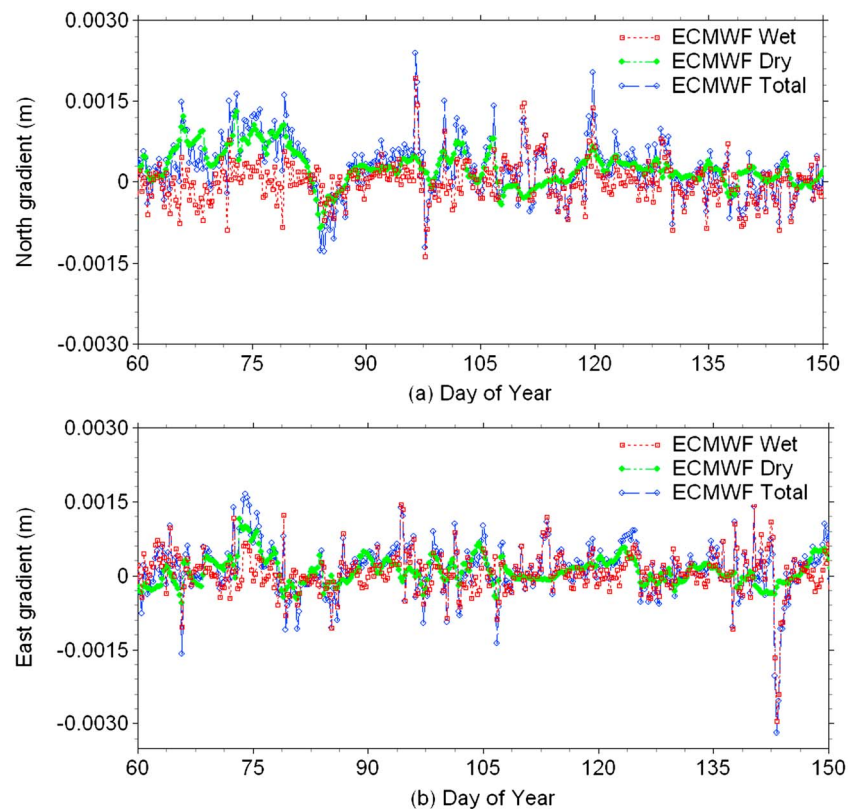


Figure 4. Tropospheric horizontal gradients retrieved from ECMWF at the GNSS station ONS1 for a period of 3 months (March, April, and May, day of year 60 to 150 in 2014). The ECMWF dry-only, wet-only, and total gradients are shown by the green, red, and blue symbols, respectively.

gradients are about 0.6, while those for GPS-only gradients are usually below 0.5. Meanwhile, the RMS values of the gradient differences are also reduced about 25–35% by multi-GNSS processing. Therefore, we conclude that the multi-GNSS fusion can provide much more accurate and stable gradient estimates with high time resolution (up to 1 h) than single-system processing. This demonstrates the significant potential of multiconstellation GNSS for meteorological applications such as numerical weather prediction and nowcasting.

4. Validations With Water Vapor Radiometer

The WVR, which is collocated with the multi-GNSS station at Onsala Geodetic Observatory (ONS1), provides us another independent technique to further validate the multi-GNSS high-resolution gradient estimates by using the WVR observations. The WVR gradients with time resolution of 1 h interval are estimated from the line-of-sight observations as described in section 2. The north gradients of 3 months retrieved from multi-GNSS and WVR are compared in Figure 3a, and the enlarged view of the period DOY 70–100 is also shown in Figure 3b to clearly observe the details. The four-system combined (GREC) solutions are shown by the green symbols, while the WVR-derived gradients are shown by the blue symbols. It can be observed that the multi-GNSS gradients only agree well with WVR gradients in some periods, e.g., the peak period around DOY 96. Significant discrepancy is seen for some time periods, e.g., DOY 70–95 where the WVR-derived gradients were underestimated with respect to the GNSS gradients.

The disagreement between GNSS and WVR gradients may be caused by two reasons. At first, the high-elevation cutoff angle of the WVR of 20° may affect the estimated gradients. Second, unlike GNSS and ECMWF, the WVR measurements are only sensitive to wet gradients and not total gradients. In order to figure out which is the main reason, we first retrieve the tropospheric gradients from ECMWF with an elevation cutoff angle of 20° instead of 3° and find small impact on the estimated gradients (see Figure S1 in the supporting information). Then we retrieve the dry-only and wet-only gradients from ECMWF and plot them in Figure 4 together with the retrieved total gradients from ECMWF. It can be seen that the slow

changes of gradients are driven by the dry part, and the fast-changing peaks are caused by the wet component. The differences between GNSS and WVR gradients shown in Figure 3 are remarkable close to the trend of the ECMWF dry gradient suggesting that the differences between GNSS and WVR gradients are caused by the inability of the WVR to estimate total gradients. Therefore, we correct the WVR wet gradients with the ECMWF dry gradients to derive total gradients. The ECMWF dry gradients of 6 h interval are linearly interpolated to be consistent with WVR gradients of 1 h interval, thanks to its smooth variation. The derived total gradients, which are labeled as WVR total, are shown in Figure 3 by the red symbols. It can be seen that the consideration of dry component improve the WVR/GNSS comparison noticeably. The multi-GNSS high-resolution gradients agree quite well with the WVR total gradients.

The east gradients of the corresponding 3 months are compared in Figure 3c, and the enlarged view of the period DOY 120–150 is shown in Figure 3d. Excellent agreement between multi-GNSS and WVR total gradients in the east component can also be clearly observed. The correlation coefficients between the GPS-only and WVR total gradients are 0.52 and 0.61 in the north and east components, respectively. The multi-GNSS processing increase the correlation coefficients to 0.63 and 0.78, corresponding to 21.2% and 27.9% improvement, respectively. The RMS values of the gradient differences are also reduced from 0.58 and 0.49 mm to 0.45 and 0.35 mm, respectively, in north and east components.

The WVR validations further confirm the performance of the high-resolution gradient estimates from multi-GNSS combined processing. In addition, it should be noticed that the dry gradients have to be corrected in the GNSS and WVR comparisons. The dry gradients derived from ECMWF are accurate enough for such corrections.

5. Conclusions

In this study, we retrieved high-resolution tropospheric gradients from multi-GNSS observations based on PPP technique. The multi-GNSS data from the IGS MGEX stations are processed, and the retrieved tropospheric gradients were compared with those derived from ECMWF and WVR as independent validations. The comparisons show that the multi-GNSS high-resolution gradients agree quite well with the ECMWF gradients, especially for spike-shaped peaks which were mostly associated with synoptic fronts. Compared to the GPS-only gradients, the high-resolution gradient estimates with multi GNSS processing are much more stable and sudden jumps observed in GPS-only solutions are significantly reduced. The multi-GNSS fusion can significantly increase the correlation coefficients of high-resolution gradient estimation to about 0.6, while those between GPS-only and ECMWF gradients are usually below 0.5. An improvement of about 20–35% is achieved by the multi-GNSS processing. The RMS values of the gradient differences are also reduced to about 25–35% by multi-GNSS processing.

After the consideration of dry component, the WVR and GNSS comparison is improved noticeably, and excellent agreement between multi-GNSS and WVR total gradients can be achieved. The correlation coefficients between the multi-GNSS and WVR total gradients are 0.63 and 0.78, respectively, in the north and east components, corresponding to 21.2% and 27.9% improvement relative to GPS-only estimates. The RMS values of the gradient differences are also reduced from 0.58 and 0.49 mm to 0.45 and 0.35 mm, respectively, in north and east components. The WVR validations further demonstrate the benefit of multi-GNSS fusion to high-resolution tropospheric gradients. The performance is expected to be further improved as more satellites will be in the sky in the next few years. Therefore, we recommend upgrading more GPS-only networks to multi-GNSS networks to exploit potential of high-resolution horizontal gradients for meteorological application such as data assimilation for short-term forecast and nowcasting of severe precipitation.

References

- Bar-Sever, Y. E., P. M. Kroger, and J. A. Borjesson (1998), Estimating horizontal gradients of tropospheric path delay with a single GPS receiver, *J. Geophys. Res.*, 103(B3), 5019–5035, doi:10.1029/97JB03534.
- Bevis, M., S. Businger, T. Herring, C. Rocken, R. Anthes, and R. Ware (1992), GPS meteorology: Remote sensing of atmospheric water vapor using GPS, *J. Geophys. Res.*, 97, 15,787–15,801, doi:10.1029/92JD01517.
- Böhm, J., A. Niell, P. Tregoning, and H. Schuh (2006), Global mapping function (GMF): A new empirical mapping function based on numerical weather model data, *Geophys. Res. Lett.*, 33, L07304, doi:10.1029/2005GL025546.
- Chen, G., and T. A. Herring (1997), Effects of atmospheric azimuth asymmetry on the analysis of space geodetic data, *J. Geophys. Res.*, 102(B9), 20,489–20,502, doi:10.1029/97JB01739.

Acknowledgments

Thanks go to the International GNSS Service (IGS) for providing multi-GNSS data. The data are available at <ftp://cddis.gsfc.nasa.gov/gnss/data/campaign/mgex/>. The Integrated Forecast System analysis data are provided by the ECMWF (<http://www.ecmwf.int/en/forecasts/datasets/dataset-i-i-atmospheric-fields-high-resolution-forecast>). We also want to thank Gunnar Elgered and Peter Forkman for the WVR data from the Onsala Geodetic Observatory. This study was partly supported by National Natural Science Foundation of China (grant 41474025).

The Editor thanks Jan Dousa for his assistance in evaluating this paper.

- Davis, J. L., G. Elgered, A. E. Niell, and C. E. Kuehn (1993), Ground-based measurement of gradients in the "wet" radio refractivity of air, *Radio Sci.*, 28(6), 1003–1018, doi:10.1029/93RS01917.
- Dousa, J., and P. Vlacovic (2014), Real-time zenith tropospheric delays in support of numerical weather prediction applications, *Adv. Space Res.*, 53(9), 1347–1358.
- Elgered, G., and P. O. J. Jarlemark (1998), Ground-based microwave radiometry and long-term observations of atmospheric water vapor, *Radio Sci.*, 33(3), 707–717, doi:10.1029/98RS00488.
- Fang, P., M. Bevis, Y. Bock, S. Gutman, and D. Wolfe (1998), GPS meteorology: Reducing systematic errors in geodetic estimates for zenith delay, *Geophys. Res. Lett.*, 25, 3583–3586, doi:10.1029/98GL02755.
- Gendt, G., G. Dick, C. Reigber, M. Tomassini, Y. Liu, and M. Ramatschi (2004), Near real time GPS water vapor monitoring for numerical weather prediction in Germany, *J. Meteorol. Soc. Jpn.*, 82, 361–370.
- Karabatic, A., R. Weber, and T. Haiden (2011), Near real-time estimation of tropospheric water vapour content from ground based GNSS data and its potential contribution to weather now-casting in Austria, *Adv. Space Res.*, 47, 1691–1703.
- Li, X., M. Ge, H. Zhang, and J. Wickert (2013), A method for improving uncalibrated phase delay estimation and ambiguity-fixing in real-time precise point positioning, *J. Geod.*, 87(5), 405–416.
- Li, X., G. Dick, M. Ge, S. Heise, J. Wickert, and M. Bender (2014), Real-time GPS sensing of atmospheric water vapor: Precise point positioning with orbit, clock and phase delay corrections, *Geophys. Res. Lett.*, 41, 3615–3621, doi:10.1002/2013GL058721.
- Li, X., X. Zhang, X. Ren, M. Fritsche, J. Wickert, and H. Schuh (2015a), Precise positioning with current multi-constellation Global Navigation Satellite Systems: GPS, GLONASS, Galileo and BeiDou, *Sci. Rep.*, 5, 8328, doi:10.1038/srep08328.
- Li, X., M. Ge, X. Dai, X. Ren, M. Fritsche, J. Wickert, and H. Schuh (2015b), Accuracy and reliability of multi-GNSS real-time precise positioning: GPS, GLONASS, BeiDou, and Galileo, *J. Geod.*, doi:10.1007/s00190-015-0802-8.
- Meindl, M., S. Schaer, U. Hugentobler, and G. Beutler (2004), Tropospheric gradient estimation at CODE: Results from global solutions, *J. Meteorol. Soc. Jpn.*, 82, 331–338, doi:10.2151/jmsj.2004.331.
- Miyazaki, S., T. Iwabuchi, K. Heki, and I. Naito (2003), An impact of estimating tropospheric delay gradients on precise positioning in the summer using the Japanese nationwide GPS array, *J. Geophys. Res.*, 108(B7), 2335, doi:10.1029/2000JB000113.
- Montenbruck, O., P. Steigenberger, R. Khachikyan, G. Weber, R. B. Langley, L. Mervart, and U. Hugentobler (2014), IGS-MGEX: Preparing the ground for multi-constellation GNSS science, *Inside GNSS*, 9(1), 42–49.
- Poli, P., P. Moll, F. Rabier, G. Desroziers, B. Chapnik, L. Berre, S. B. Healy, E. Andersson, and F.-Z. E. Guelai (2007), Forecast impact studies of zenith total delay data from European near real-time GPS stations in Météo France 4DVAR, *J. Geophys. Res.*, 112, D06114, doi:10.1029/2006JD007430.
- Rocken, C., T. Van Hove, and R. Ware (1997), Near real-time sensing of atmospheric water vapor, *Geophys. Res. Lett.*, 24, 3221–3224, doi:10.1029/97GL03312.
- Saastamoinen, J. (1973), Contributions to the theory of atmospheric refraction—Part II. Refraction corrections in satellite geodesy, *Bull. Géod.*, 47(1), 13–34, doi:10.1007/BF02522083.
- Shoji, Y. (2013), Retrieval of water vapor inhomogeneity using the Japanese nationwide GPS array and its potential for prediction of convective precipitation, *J. Meteorol. Soc. Jpn.*, 91, 43–62.
- Zumberge, J. F., M. B. Heflin, D. C. Jefferson, M. M. Watkins, and F. H. Webb (1997), Precise point positioning for the efficient and robust analysis of GPS data from large networks, *J. Geophys. Res.*, 102(B3), 5005–5017, doi:10.1029/96JB03860.
- Zus, F., G. Dick, J. Dousa, S. Heise, and J. Wickert (2014), The rapid and precise computation of GPS slant total delays and mapping factors utilizing a numerical weather model, *Radio Sci.*, 49, 207–216, doi:10.1002/2013RS005280.